International Journal of New Horizons in Physics

http://dx.doi.org/10.18576/ijnhp/100101

Investigation of dilute Gd doped ZnO film: structural and morphological properties for various applications

A. Z. Mahmoud[1,2], E. M. M. Ibrahim[3], Lamiaa Galal[2,3,4], and E. R. Shaaban[5,]*

[1]Physics Department, College of Sciences and Art At ArRass, Qassim University, ArRass 51921, Kingdom of Saudi Arabia
[2]Physics Department, Faculty of Science, Assiut University, Assiut, Egypt
[3]Physics Department, Faculty of Science, Sohag University, Sohag 82524, Egypt
[4]Physics Department, Faculty of Science, Northern Border University, Arar 91431, Saudi Arabia
[5]Physics Department, Faculty of Science, Al-Azhar University, Assiut, 71542, Egypt

Received: 2 Aug. 2022, Revised: 4 Dec. 2022, Accepted: 8 Dec. 2022
Published online: 1 Jan. 2023

Abstract: The co-precipitation process is used to create various compositions of the bulk sample of $Zn_{1-x}Gd_xO$ (x = 0, 0.02, 0.04, 0.06, 0.08, and 0.1). The current study examines the morphological and structural characteristics of Gd-doped ZnO thin films. By using an electron beam approach, the required coatings were deposited onto extremely clean glass substrates. The production of the hexagonal wurtzite single phase of ZnO, which exhibits a strong (002) peak with a peak shift towards lower angle, was discovered by X-ray diffraction. It was discovered that the films' crystallite sizes shrank as the Gd content rose. Calculations have been made for the lattice constant, cell volume, atomic packing fraction, and surface density. $Zn_{1-x}Gd_xO$ thin films' microstructural characteristics, crystallite size, and lattice strain were computed. Zn1-xGdxO thin films' microstructural characteristics, crystallite size, and lattice strain were computed. The details of the alterations in microstructural parameters in relation to Gd concentration were then covered. $Zn_{1-x}Gd_xO$'s Zn-O bond lengths and bond angles were established and have since changed. The turnability of microstructural parameters recommend $Zn_{1-x}Gd_xO$ samples in various applications in electronic devices.

Keywords: Gd doped ZnO, Structure parameters, Bond length, Bond angle, SEM.

1 Introduction

Wide band gap (3.37 eV) with high exciton binding energy (60 meV), low dielectric constant, good chemical stability, high electrochemical coupling coefficient, high thermal conductivity, and UV protection are just a few of the intriguing characteristics of ZnO [1-3]. ZnO films have a wide range of applications due to their high refractive index and high transmittance in the visible and infrared spectrum ranges. Due to their distinctive electrical, magnetic, and magneto-optical features, diluted magnetic semiconductors (DMS) have recently gained attention [4, 5].

By adjusting the lattice parameters, microstructural parameters, and energy gaps in relation to the concentration of transition metal (TM), their structural, electrical, and optical properties can be changed [6, 7]. The creation of repeatable long-range ferromagnetism (FM) in materials with a large bandgap-DMS remains a significant barrier, however, to the creation of spintronic devices that operate above room temperature [7, 8]. Some experimental experiments have demonstrated that rare earth (RE) doping of metals, such as doping GaN with the ion Gd^{3+}, can enhance the ferromagnetic characteristic [9]. This encourages researchers to dope metal oxide materials with RE metal ions for spintronics applications. Due to its scintillation and optical devices instead of other luminescent and magnetic materials, Gd^{3+} is of particular interest [10–12].

Compared to ZnO doped with transition metals, Gd-doped ZnO can create FM that is stronger. This difference may be caused by a disputed interaction between localised 4f electrons and host electrons. The crystal defect caused by the rare earth doping of ZnO has been implicated in ferromagnetism [13, 14]. The benefits of Gd-doped ZnO are numerous. Because holes in 4f Gd are more active than electrons, it has been claimed that Gd ions doped into ZnO increase hole conductivity [15]. Additionally, it has been discovered that Gd doped ZnO possesses an enormous magnetic moment at ambient temperature [16] that can be exploited to create ZnO-based spin electrical devices. The domains of light-emitting displays, catalysis, drug delivery, and optical storage are thought to have substantial promise for Gd doped ZnO

*Corresponding author e-mail: esam_ramadan2008@yahoo.com

nanoparticles [17].

In our work, we prepared $Zn_{1-x}Gd_xO$ (x = 0, 0.02, 0.04, 0.06, 0.08 and 0.1) thin films on a glass substrate with a fixed thickness (200 nm). Morphology of the films has been investigated by various structural parameters e.g., Lattice constant, Cell volume, Atomic Packing Fraction and surface density have been calculated. The microstructural parameters, crystallite size and lattice strain of $Zn_{1-x}Gd_xO$ thin films were calculated. The analysis indicates that the $Zn_{1-x}Gd_xO$ thin films were uniformly distributed with smooth grain boundaries. Comparison of these parameters of all ZnO films with different dilute Gd content leads to in-depth understanding of various physical properties that depends on surface morphology and structural parameters for varies applications.

2 Experimental

The co-precipitation technique of Zn $(NO_3)_2.6H_2O$ with the appropriate amount of Gd $(NO_3)_3.6H_2O$ to make the required doping percentage dissolved in 50 ml of distilled water was used to make different compositions of bulk samples of $Zn_{1-x}Gd_xO$ (x = 0, 0.02, 0.04, 0.06, 0.08, and 0.1). In deionized water, zinc and gadolinium nitrates are dissolved and stirred for 1 hour. The NH_4OH solution was added dropwise till the PH of the solution had reached 9. This mixture was stirred for 2 hours at room temperature and, consequently, filtered. The precipitate was dried for 4 hours at 80 degrees Celsius.

The precursor underwent thermogravimetric analysis (TGA) using a Shimadzu 50. A polycrystalline powder was obtained by calcining the material at 450 ºC for two hours, as determined by TGA analysis. Using the electron beam gun approach, different $Zn_{1-x}Gd_xO$ thin films of equal thickness were evaporated under a vacuum of around 10-6 Pa. A quartz crystal FTM6 monitor was used to regulate the evaporation rate and film thickness. Throughout the production of the sample, the deposition rate was kept constant at 2 nm/s approximately. A film with a composition that is nearly identical to the bulk starting material can be created at such a low deposition rate.

$Zn_{1-x}Gd_xO$ powder and thin films' structural characteristics were examined using X-ray diffraction (XRD; Shimadzu X-ray diffractometry 6000, Japan) and Cu-K radiation with a wavelength of 0.15418 nm. Step scan modes with a 2 range between 5 and 70º, a step size of 0.02º, and a step period of 0.6 s were used to gather the intensity data. As an internal standard, pure silicon (Si 99.9999%) is employed. Energy-dispersive X-ray (EDX) spectrometer energy-dispersive analysis of X-ray (EDAX) is used to determine the composition of the produced polycrystalline particles. The morphology of the films was examined using scanning electron microscopy (SEM), and several structural parameters, such as the lattice constant, cell volume, atomic packing fraction, and surface density, were calculated.

3 Results and discussion

To research the thermal behaviour of precursor materials, one of the most important thermal analysis techniques is TGA. As depicted in Fig. 1, TGA was performed at temperatures ranging from ambient temperature to 700 °C. According to this number, a weight loss of almost 17% was connected to the three phases that came after the first, which happened until 361°C and was caused by the elimination of water that had been adsorbed on the material's surface. The complete crystallisation of zinc oxide from its amorphous state may be responsible for the second weight loss of approximately 7% that happened between 361°C and 450°C. The oxidation of residual chemicals causes the third weight loss, which amounts to 2%.

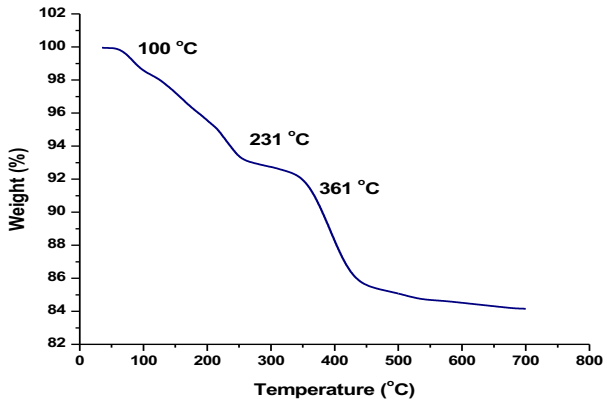

Fig. 1: Thermogravimetric analysis of the precursor.

3.1 Energy-dispersive analysis X-ray (EDAX) spectra

EDAX can be used to locate peaks that correlate to the movie's constituents. The more concentrated an element is in the spectrum, the higher its peak appears. In Fig. 2 EDAX data illustrates the Zn and Gd atoms present in the prepared $Zn_{0.94}Gd_{0.06}O$ film. The purity of the film sample is confirmed by the lack of additional components in the spectra.

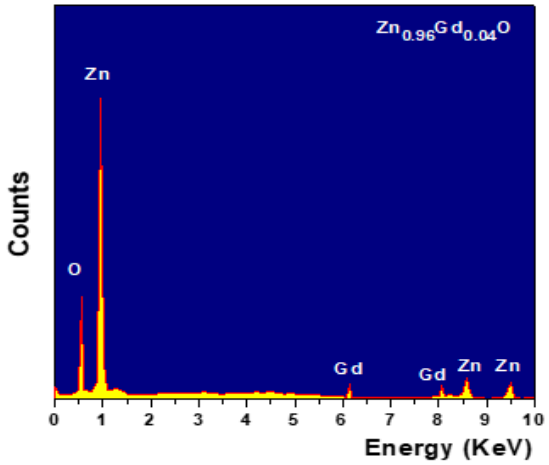

Fig. 2: Energy-dispersive analysis of X-ray spectra $Zn_{0.96}Gd_{0.04}O$ thin film.

3.2 XRD analysis

Figure 3 displays the X-ray diffraction patterns of the as-deposited ZnO and the Gd-doped ZnO in the $Zn_{1-x}Gd_xO$ thin films. Thin $Zn_{1-x}Gd_xO$ film patterns were compared to typical JCPDS data. The hexagonal wurtzite ZnO structure (JCPDS 01-1136) is properly indexed to all of the diffraction peaks, demonstrating that the doping of Gd has no effect on the crystal structure of ZnO. The production of the $Zn_{1-x}Gd_xO$ solid is confirmed by the XRD pattern's lack of Gd traces or any other impurity phase diffraction peaks. Additionally, Fig. 3 demonstrates that when Gd concentration rises, the intensity of the favoured orientation (002) plane peaks weakens and shifts towards lower values of the diffraction angle (see Fig. 4)

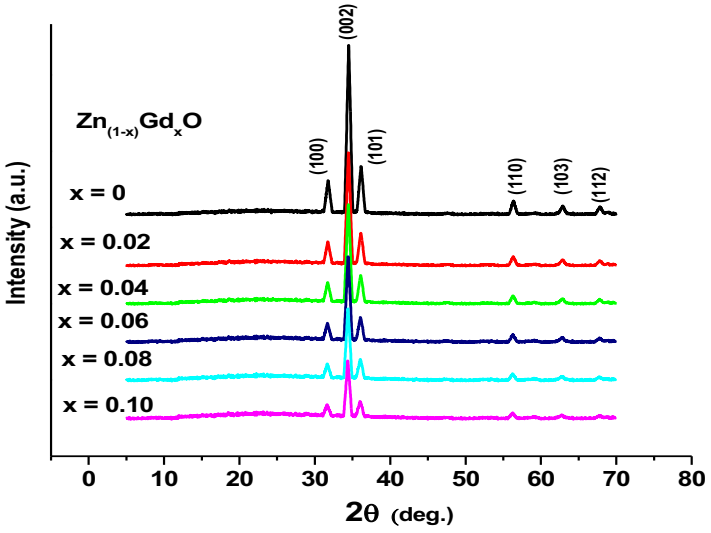

Fig. 3: X-ray diffraction patterns of polycrystalline $Zn_{1-x}Gd_xO$ thin films.

Since the ionic radii of Gd^{3+} ions are greater than those of Zn^{2+} ions (r = 0.074 nm), the peak position has shifted by 0.0938. Additionally, as seen in table 2, the full width at half maximum (FWHM) increases with increasing Gd content. This behaviour suggests that the crystallite size and, consequently, the crystalline quality of the thin films have decreased. Scherrer's formula can be used to determine the crystallite size (D) [18, 19]:

$$D = \frac{0.9\lambda}{\beta \cos\theta} \tag{1}$$

The difference between the sample's integral X-ray peak profile width and a standard (silicon) is given by, $\beta = \sqrt{\beta_{obs}^2 - \beta_{std}^2}$ and λ is the incident wavelength

Table 2 demonstrates that as the Gd concentration rises, the D values fall. The formation of oxygen vacancies with Gd ions, which lower the lattice properties and produce a significant tensile stress, is what causes the drop in crystallite size [20]. Additionally, the Gd dopant's inclusion prevents the ZnO particles from adhering together, which reduces the average crystallite size [21].

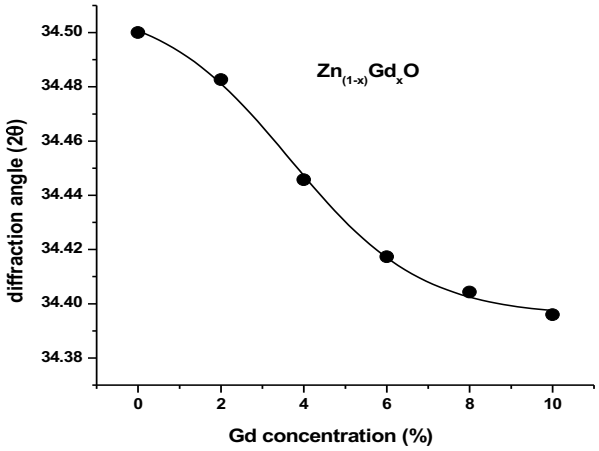

Fig. 4: Diffraction angles as a function of Gd concentration for $Zn_{1-x}Gd_xO$ thin films.

Table 1: Morphological parameters of $Zn_{1-x}Gd_xO$ thin films.

Conc. x %	a (Å)	c (Å)	c/a	V (Å)3	ε_a	ε_c
0	3.01524	5.07987	1.68473	39.9969	0.00048	0.03321
2	3.01609	5.09155	1.68813	40.1115	0.00076	0.03558
4	3.01865	5.101	1.68983	40.2542	0.00161	0.03751
6	3.02122	5.10688	1.69034	40.3691	0.00246	0.0387
8	3.02379	5.11276	1.69085	40.4844	0.00332	0.0399
10	3.02636	5.11763	1.69102	40.592	0.00417	0.04089

3.3 The lattice parameters

The plane spacing equation can be used to determine the lattice parameters 'a' and 'c' of the wurtzite structure of ZnO and Gd-doped ZnO films [22].

$$\frac{1}{d_{hk\ell}^2} = \frac{4}{3}\left(\frac{h^2 + hk + k^2}{a^2}\right) + \frac{\ell^2}{c^2} \tag{3}$$

Where a & c are the lattice parameters, d is the interplanar distance and (hkl) are the Miller indices with the first-order approximation (n = 1) for the (100) plane and using the Bragg equation $n\lambda = 2d_{hk\ell}sin\theta$ The lattice parameter 'a' and 'c' is obtained from the relations.

Using the first-order approximation (n = 1) for the (100) plane and the Bragg equation, $n\lambda = 2d_{hk\ell}sin\theta$, the lattice parameters a and c, the interplanar distance d, and the Miller indices (hkl), The relations are used to derive the lattice parameters "a" and "c."

$$a = \frac{\lambda}{(\sqrt{3}\sin\theta_{100})} \quad \& \quad c = \frac{\lambda}{\sin\theta_{002}} \tag{4}$$

The quality of the ZnO thin films is shown by the values of the lattice parameters "a" and "c," which are in good agreement with the benchmark values for ZnO single crystals (a = 3.250 and c = 5.207). As strong markers of compressive stress in the films, the values of the lattice parameters "a" and "c" are lower than those of bulk doped films [23]. Table 1 shows that the lattice parameters "a" and "c" rise when the Gd concentration of Zn1-xGdxO increases. The geometry of ZnO and Gd doped ZnO wurtzite structures is fairly excellent, as seen by the lattice parameter c/a ratio, which is almost equal to 1.6. Table 1 contains the values of the lattice parameters "a," "c," and c/a.

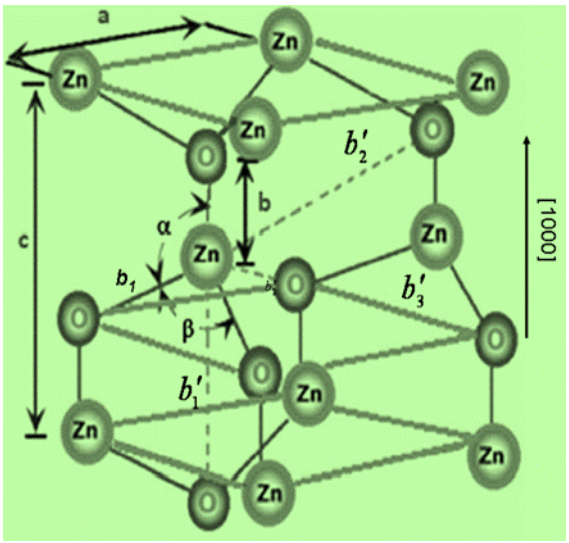

Fig. 5: Unit cell of ZnO.

3.4 Atomic Packing Fraction (APF)

It is defined as the portion of volume occupied by constituent particles in a crystal structure. It is an indivisible amount that is perpetually smaller than unity. Using the formula [24], the atomic packing fraction (APF) for hexagonal was computed.

$$P = \frac{2\pi a}{3c\sqrt{3}} \tag{5}$$

where "a" and "c" are lattice parameters [25]. The findings indicate that the APF declines with Gd content, which might be because there are less voids in the samples. The APF of hexagonal ZnO in bulk is around 75%, however in this study, the APF of the $Zn_{1-x}Gd_xO$ film is more than 75%, suggesting that the APF in the nanocrystals is a little higher than that in the bulk material. Size effects in nanocrystalline thin films are responsible for this. The APF in $Zn_{1-x}Gd_xO$ films decreases as Gd concentration increases, showing consistent Gd ion substitution in the zinc sites of the ZnO structure [26]. Table 2 contains the atomic packing fractions (APFs) of the $Zn_{1-x}Gd_xO$ films.

Table 2: Crystallite size, lattice strain, dislocation density, X-ray density, packing factor and surface energy respectively for $Zn_{1-x}Gd_xO$ thin films.

Conc. x %	Corrected β	D (nm)	ε	δ x 10-4 (nm)-2	ρ (g/cm3)	P	S (cm2/g)
0	0.1971	44	0.0028	52	6.7573	71.7739	20.2
2	0.2258	38	0.0032	68	6.738	71.6295	23.2
4	0.2488	35	0.0035	82	6.7141	71.5575	25.6
6	0.2702	32	0.0038	97	6.695	71.536	27.9
8	0.2875	30	0.0041	110	6.676	71.5144	29.8
10	0.3067	28	0.0044	125	6.6583	71.5072	31.8

3.5 Volume of unit cell and X-ray density

The unit cell volume was computed using the equation [27]

$$V = \frac{\sqrt{3}}{2} a^2 c \tag{6}$$

Here the lattice parameters *a* and *c*. The values of the unit cell volume are provided in Table 1, and it is discovered that the unit cell volume rises with rising Gd concentration, which can be attributed to the rise in lattice parameters a and c. This implies that the Gd ions have relocated to the structure's available zinc sites.

The number of unit cells in the particle is calculated from the equation [28]

$$N = \frac{4}{3\pi \frac{D}{2V}} \tag{7}$$

The X-ray density of ZnO sample was calculated by using the formula [29]

$$\rho = \frac{nM}{N_A V} \tag{8}$$

Where M is the sample's molecular weight, n is the number of atoms per unit cell, and ρ is the X-ray density The Avogadro number is NA, while the unit cell's volume is V. With increasing Gd content in $Zn_{1-x}Gd_xO$ nanoparticles, the X-ray density rises. This might be caused by an increase in sample molecular weight and unit cell capacity. The unit cell volume increases and the X-ray density falls as the Gd content rises. In the ZnO structure, this implies that Gd ions reach the Zn sites [30].

3.6 Specific surface area

It is a solids attribute that can be used to identify a material's nature and properties. It is defined as the total surface area of a material per unit of mass. The measurement method affects the results found for a particular area. The particle size provided by [31] can be used to compute the specific surface area.

$$S = \frac{6x\ 10^8}{Dx\ \rho} \tag{9}$$

The specific surface area decreases with iron incorporated as shown in Table 2.

From this study, the dislocation density (δ) and crystallize size of estimated samples are calculated by using following equation:

$$\delta = \frac{1}{D^2} \tag{10}$$

Any material's dislocation density determines the quality of its films and its defect structure. The number of dislocations per unit length or per unit area of the desired samples is the standard definition of the dislocation density. As Gd is added to the ZnO matrix in the current work, the dislocation density steadily rises, revealing the defect structure. The formulas c =((c-c_o) c)100% and a =((a-a_o) a)100% can be used to compute the strain in both the c- and a- axis directions. The data are given in Tables 2 and 1, respectively, for δ and "ε_c, ε_a".

The lattice strain (ε) can be calculated from Stoke and Wilson Eq. [32]

$$\varepsilon = \frac{\beta_{Strain}}{4tan\theta} \tag{11}$$

Where, K is the shape factor, which is a constant taken as 0.94 λ is the wavelength of the X-ray radiation (λ=1.5416 Å), θ is the Bragg's angle in degree and β is the full width at the half maximum (FWHM) of the prepared films. The crystallite size decreases with increasing Gd incorporation, but the lattice strain increases. Both trend of D and ε may attribute to the change in the lattice size with Gd substitution by Zn because the ionic radius of Gd (Gd^{3+}: 0.094 nm) is slightly smaller the ionic radius of Zn (Zn^{2+}: 0.074 nm) for the same coordination number (four-fold coordination). The observed decrease in D and increases in lattice strain can be attributed to the combined effects of I the host ZnO crystal's lattice distortion caused by the substitution of smaller ionic-sized iron atoms [33] and (ii) the obstruction of crystal growth caused by the development of a thin layer of Gd-O-Zn on the surface of the doped samples as a result of the presence of too many iron ions in the precipitation solution [34].

3.7 Bond length and bond angle

Different atoms all combine with each other and become stable. This bonding is achieved by forming bonds. There are different types of bonds, namely ionic or electrovalent bonds, covalent bonds and coordinate bonds. This in turn indicates that each bond is associated with a specific property. Bond length describes the distance between the nucleus centers of two bonded atoms in equilibrium. The stronger the attraction between the bonded atoms, the smaller the bond length. However, the larger the atomic size, the longer the bond length. Bond angle refers to the angle between two bonds, that is, the angle between two orbitals that contain a pair of bonding electrons around the central atom of a complex molecule or ion.

The Zn–O bond length L is given by [35]

$$L = \sqrt{\left(\frac{a^2}{3} + c^2\left(\frac{1}{2}\text{-}u\right)^2\right)} \tag{14}$$

where a and c are lattice parameters, u is the positional parameter in the wurtzite structure and measures the amount which each atom gets displaced with respect to the next [36]. and u is given by

$$u = \frac{a^2}{3c^2} + \frac{1}{4} \tag{15}$$

While the stated Zn-O bond length in the unit cell of ZnO and adjacent atoms is 1.9767, the Zn-O bond length computed according to this work ranges from 1.8665 to 1.8759. The estimated and actual bond lengths are in good agreement, supporting the findings of the current investigation. Table 3 provides the bond length value.

In additional, there are three types of second-nearest neighbors, which designated as b_1' (one along the direction), b_2' (six of them) and b_3' (three of them) with the bond lengths, shown in Fig. 6 are calculated as [38]

$$b_1' = c(1\text{-}u) \tag{16}$$

$$b_2' = \sqrt{a^2 + (uc)^2} \tag{17}$$

$$b_3' = \sqrt{\frac{4a^2}{3} + (\frac{1}{2} - u)^2 c^2} \tag{18}$$

The second-nearest neighbours are less distant when the Gd doping concentration rises. The higher occupancy of the dopant is to blame for this. Table 3 shows how the second-nearest neighbour varies with Gd doping concentration. It's interesting to note that for Wurtzite geometry, the two distances, b_2 and b_3, are equivalent. The bond angles are given by,

$$\alpha = \frac{\pi}{2} + cos^{-1}\left[1 + 3\left(\frac{c}{a}\right)\left(-u + \frac{1}{2}\right)^2\right]^{-1} \tag{19}$$

$$\beta = 2sin^{-1}\left[\frac{4}{3} + 4\left(\frac{c}{a}\right)^2\left(-u + \frac{1}{2}\right)^2\right]^{-1} \tag{20}$$

The estimated bond angles match the reference value (= 109.47) exactly. For the best scenario, the ratio between and is one. However, regardless of the Gd doping concentration, the ratio for Gd doped ZnO nanoparticles is 1.03. Table 3 displays each of the evaluated values.

Table 3: The Values of Positional parameter, bond length and bond angle for undoped and Gd doped ZnO.

Conc. x%	u	b (Å)	b_1' (Å)	b_2' (Å)	b_3' (Å)	α (°)	β (°)
0	0.3674401	1.866548	3.213322	3.546217	3.546217	111.1472	107.7444
2	0.366968	1.868436	3.223115	3.547936	3.547936	111.2548	107.6302
4	0.366733	1.870705	3.230296	3.551308	3.551308	111.3085	107.5731
6	0.3666626	1.8725	3.234375	3.554434	3.554434	111.3246	107.5559
8	0.3665923	1.874298	3.238461	3.557566	3.557566	111.3407	107.5388
10	0.3665689	1.875963	3.241664	3.560631	3.560631	111.3461	107.5331

3.8 Scanning Electron Microscopy (SEM)

The surface morphologies of the films are shown in Fig. 6. In general, the size of the nanoparticles is homogenous, but variable concentrations result in porous granular surfaces. Figure 6(a) illustrates how the size of the nanoparticles almost forms a sphere. The size of the nanoparticles shrank into smaller cluster grains as the Gd concentration was raised, as illustrated in Fig. 6. (b-e).

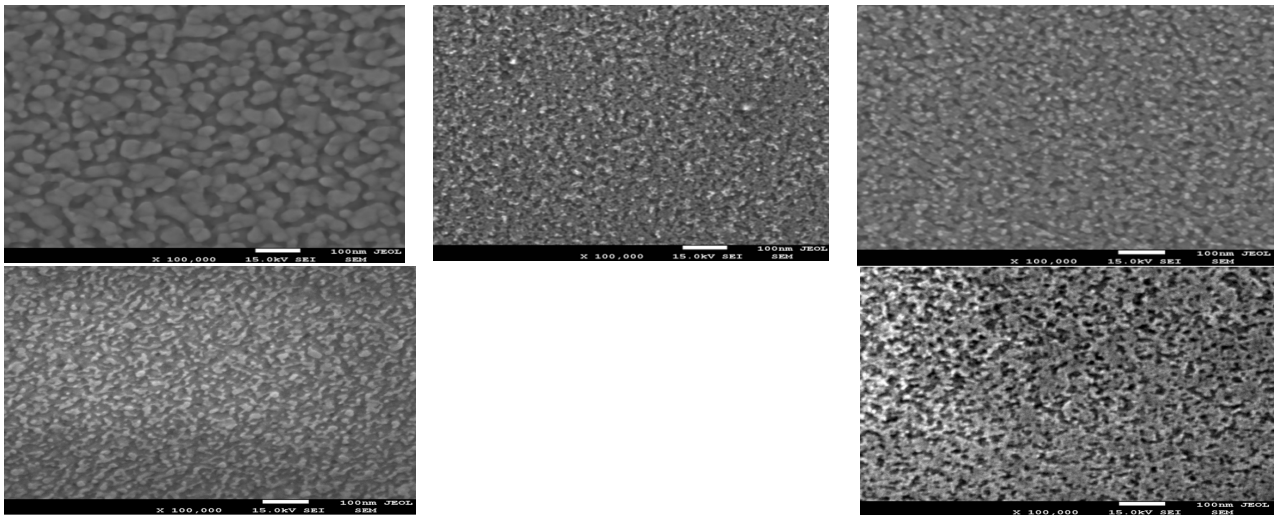

Fig. 6: SEM micrographs of $Zn_{1-x}Gd_xO$ thin films with (x = 0, 0.02, 0.04, 0.06 and 0.08mol.).

4 Conclusions

In this study, the bulk sample of $Zn_{1-x}Gd_xO$ was prepared using the co-precipitation process in various compositions (x = 0, 0.02, 0.04, 0.06, 0.08, and 0.1) before being deposited as thin films using the electron beam approach on extremely clean glass substrates. In-depth research was done on the structural and morphological characteristics of thin Gd-doped ZnO films. The films demonstrate the emergence of the intense (002) peak in the hexagonal wurtzite single phase of ZnO, with the peak shifting towards a lower angle. With increasing Gd concentration from 0 to 0.1, it was discovered that the crystallite size of the films fell from 44 nm to 28 nm. Based on the structural modification, which further improves upon Gd-doping, the changes in the Bond length and Bond angle of the prepared films were discussed. For the first time, the second-nearest neighbour distances for Gd doped ZnO nanoparticles were computed. Microstructural characteristics' turnability suggests using $Zn_{1-x}Gd_xO$ samples for a variety of electronic device applications.

References

[1] M. Bouloudenine, N. Viart, S. Colis, J. D. Kortus, *Appl. Phys. Lett.* **87** (2005) 052501.
[2] A. S. Risbud, N. A. Spaldin, Z. Q. Chen, S. S. Stemmer, *Phys. Rev. B* **68** (2003) 205202.
[3] S. Thota, T. Dutta, J. Kumar, *J. Phy.s: Condens. Matter.* **18** (2006) 2473.
[4] S. J. Pearton, C. R. Abernathy, M. E. Overberg, G. T. Thaler, D. P. Norton, *J. Appl. Phys.* **93** (2003) 1.
[5] X. Wang, J. Xu, B. Zhang, H. Yu, J. Wang, X. Zhang, J. Yu, Q. Li, *Adv. Mater.* **18** (2006) 2476.
[6] G. Vijayaprasath, R. Murugan, T. Mahalingam, Y. Hayakawa, G. Ravi, *Ceram. Int.* **41** (2015) 10607–10615.
[7] G. A. Prinz, *Science* **282** (1998) 1660.
[8] S. Chambers, *Nat. Mater.* **9** (2010) 956.
[8] G. Vijayaprasath, R. Murugan, T. Mahalingam, Y. Hayakawa, G. Ravi, *J. Alloys Comp.,* **649** (2015) 275.
[9] S. Dhar, O. Brandt, M. Ramsteiner, V. F. Sapega, K. H. Ploog, *Phys. Rev. Lett.,* **94**
(2005) 037205.
[10] J. S. Bae, J. H. Jeong, S. S. Yi, J. C. Park, *Appl. Phys. Lett*. **82** (2003) 3629.
[11] C. D. Pemmaraju, R. Hanafin, T. Archer, H. B. Braun, S. Sanvito, *Phys. Rev. B* **78** (2008) 054428.
[12] H. Gu, Y. Jiang, Y. Xu, M. Yan, *Appl. Phys. Lett.* **98** (2011) 012502.

[13] X.-L. Li, J.-F. Guo, Z.-Y. Quan, X.-H. Xu, G. A. Gehring, *IEEE Trans. Magn.* **46** 1382 (2010) 1382.
[14] C. J. Cong, L. Liao, Q. Y Liu, J. C. Li, K. L. Zhang, *Nanotechnology* **17** (2006) 1520.
[15] L. Liu, P. Y. Yu, Z. Ma, S. S. Mao, Physical Review Letters 100 (2008) 127203
[16] A. Khodorov, A. G. Rolo, E. K. Hlil, J. Ayres de Campos, O. Karzazi, S. Levichev, M. R. Correia, A. Chahboun, M. J. M. Gomes, *Eur. Phys. J. Appl. Phys.* **57** (2012) 10301.
[17] J. Zhong, S. Muthukumar, Y. Chen, Y. Lu, H. M. Ng, W. Jiang, etal., Applied Physics Letters 83 (2003)3401.
[18] A. L. Patterson, Phys. Rev. **56** (1939) 978.
[19] E. R. Shaaban, M. El-Hagary, M. Emam-Ismail, M. B. El-Den, Philosophical Magazine 91 (12) (2011) 1679.
[20] A. A. Dakhel, M. El-Hilo, *J. Appl. Phys.* **107** (2010) 123905.
[21] A. Khataee, R. D. C. Soltani, A. Karimi, S. W. Joo, *Ultrason. Sonochem.* **23** (2015) 219.
[22] E. R. Shaaban, A. Almohammedi, E. S. Yousef, G. A. M. Ali, K. F. Chong, A. Adel, A. Ashour, *Optik* **164** (2018) 527.
[23] R. Swanepoel, *J. Phys. E: Sci. Instrum.* **16** (1983) 121.
[24] E. R. Shaaban, I. S. Yahia, E. G. El-Metwally, *Acta Phys. Pol. A* **121** (2012) 628.
[25] T. Bellunato, M. Calvi, C. Matteuzzi, M. Musy, D. L. Perego, B. Storaci, *Europ. Phys. J.* **52** (2007) 759.
[26] F. A. Jenkins, H. E. White, *J. Phys. E: Sci. Instrum.* **16** (1983) 1214.

[28] E. Marquez, J. B. Ramirez-Malo, P. Villares, R. Jimenez-Garay, R. Swanepoel, *Thin Solid Films* **234** (1995) 83.

[29] Y. E. Lee, Y. J. Kim, H. J. Kim, *J. Mater. Res.* **13** (1998) 1260.
[30] H. Tabet-Derraz, N. Benramdane, D. Nacer, A. Bouzidi, M. Medles, *Sol. Energy Mater. Solar Cells.* **73** (2002) 248.
[31] L. F. Dong, Z. Cui, Z. K. Zhang, *Nanostru. Mater.* **8** (1997) 815.
[32] E. A. Davis, N. F. Mott, *Philos. Mag.* **22** (1970) 903.
[33] E. A. Davis, N.F. Mott, *Philos. Mag.* **22** (1970) 903.
[34] E. R. Shaaban, *Philos. Mag.* **88** (2008) 781.
[35] E. R. Shaaban, M. Abdel-Rahman, E. Yousef, M. T. Dessouky, *Thin Solid Films* **515** (2007) 3810.
[36] E. R. Shaaban, *Appl. Phys. A* **115** (2014) 919.
[37] E. R. Shaaban, *J. Alloys Compds*. **563** (2013) 274.
[38] M. Emam-Ismail, M. El-Hagary, E. R. Shaaban, S. Althoyaib, *J. Alloys Compds* 529 (2012) 113.